Silicon micro venturi nozzles for cost-efficient spray coating of thin organic P3HT/PCBM layers

OPEN ACCESS
IOP Publishing
Journal of Micromechanics and Microengineering
J. Micromech. Microeng. **27** (2017) 015019 (9pp)
doi:10.1088/0960-1317/27/1/015019

Silicon micro venturi nozzles for cost-efficient spray coating of thin organic P3HT/PCBM layers

Michael A Betz[1], Patric Büchele[2,3], Manfred Brünnler[1], Sonja Deml[1] and Alfred Lechner[1]

[1] Competence Center Nanochem, Faculty of General Studies and Microsystems Technology, OTH Regensburg, Seybothstraße 2, 93053 Regensburg, Germany
[2] Siemens Healthcare GmbH, Technology Center, Günther-Scharowsky-Straße 1, 91058 Erlangen, Germany
[3] Light Technology Institute and Institute of Microstructure Technology, Karlsruhe Institute of Technology, Kaiserstraße 12, 76131 Karlsruhe, Germany

E-mail: michael.andreas.betz@gmail.com

Received 4 August 2016
Accepted for publication 14 October 2016
Published 16 November 2016

Abstract

Improvements on spray coating are of particular interest to different fields of technology as it is a scalable deposition method and processing from solutions offer various application possibilities outside of typical facilities. When it comes to the deposition of expensive and film-forming media such as organic semiconductors, consumption and nozzle cleaning issues are of particular importance. We demonstrate the simple steps to design and fabricate micro venturi nozzles for economical spray coating with a consumption as low as 30–50 $\mu l \cdot min^{-1}$. For spray coating an active area of 25 cm^2 a 2.45–4.01 fold coating efficiency is observed compared to a conventional airbrush nozzle set. The electrical characterization of first diodes sprayed with an active layer thickness of ~750 nm using a single micronozzle at a coating speed of 1.7 $cm^2 \cdot min^{-1}$ reveals a good external quantum efficiency of 72.9% at 532 nm and a dark current of ~$7.4 \cdot 10^{-5}$ $mA \cdot cm^{-2}$, both measured at −2 V. Furthermore, the high resistance of the micronozzles against solvents and most acids is provided through realization in a silicon wafer with silicon dioxide encapsulation, therefore allowing easy and effective cleaning.

Keywords: deep reactive ion etching, microfluidics, organic semiconductors, organic photodiodes, spray coating, venturi nozzles

S Online supplementary data available from stacks.iop.org/JMM/27/015019/mmedia

(Some figures may appear in colour only in the online journal)

1. Introduction

The spread of organic photodiodes (OPDs) and organic photovoltaics (OPVs) is limited because silicon devices still offer higher efficiencies and are available at a lower price, partially due to mass production effects. Many research groups around the world continue to work on scalable deposition methods such as spray coating, as the benefits from solution processing and application possibilities potentially outweigh the disadvantages by far. The benefits, for example, are lattice-independent large area coating, continuous flow processing and therefore a reduction in cost per area [1]. Furthermore, spray coating enables the use of fluids with different rheologies, and leaves the user independent from substrate material and form [2]. Krebs describes spray coating as one of the coating methods compatible with roll-to-roll processing in

his review of printing and coating techniques for OPV, which we gladly recommend as overview of applicable coating methods [3]. Still, he highlights the difficulty of obtaining smooth surfaces, which will also be addressed in this paper. Another intensively discussed alternative application method is ultrasonic spray coating, which is similar to spraying with micronozzles in terms of generated droplet size and drying behavior [4], and therefore shares similar characteristics.

A promising approach to better market OPDs and OPVs is to reduce the amount of expensive organic semiconductors (OSCs) required to form the active layer. For conventional spin coating (resulting in best layer quality), more than 90% of the organic semiconductors are spun off the substrate and lost [5]. As long as OSCs such as the electron-conductor PCBM (phenyl-C61-butyric-acid-methyl-ester) cost up to 1850 €/g depending on purity [6], making them the main matter of expense, such loss rates are highly uneconomic and impede the further spread of OPDs and OPVs. By using our micronozzles the overspray shall be reduced and the coating efficiency for the spray coating OSC layers increased accordingly.

Another important issue when spray coating film-forming organic semiconductors is the guarantee of thorough nozzle cleaning as small residues may have a serious impact on the spray result, e.g. doping or reduced layer thickness. For those reasons, we realize micro venturi nozzles in a silicon wafer with silicon dioxide encapsulation allowing easy cleaning and economical spray coating without performance losses.

In this paper, we will show the design of micro venturi nozzles based on FEM (finite element method) simulations and several nozzle evaluation steps (section 2.1). We demonstrate the simple fabrication of the nozzles using a single dry etch process to structure a silicon wafer, anodic bonding with a borosilicate glass wafer to perform capping and a wafer saw for nozzle separation (section 2.2). We will picture the spray cone, drop size distribution and layer properties using profilometer scans and optical microscopy (section 3.1). We also visualize droplet dispersion and compare it to conventional airbrush technology applying a CCD-based high-speed camera (section 3.1). Furthermore, we demonstrate how to economically spray coat with a single nozzle and a 2.45–4.01 times enhanced coating efficiency (compared to the conventional airbrush nozzle set) at a speed of $1.7\,\mathrm{cm}^2 \cdot \mathrm{min}^{-1}$ only consuming 30–50 $\mu\mathrm{l} \cdot \mathrm{min}^{-1}$ of OSC chlorobenzene solution (section 3.2). Finally, we show the electrical characterization of first sprayed diodes and discuss how to further increase coating speed and improve atomization and layer homogeneity (sections 3.2 and 4).

2. Fabrication and experimental methods

2.1. Design

Our goal was to transform a basic venturi nozzle design, as e.g. described in [7], to the microscale, suitable for structuring by photolithography and dry etching (similar in setup to that presented in [8]). In order to achieve sufficient venturi suction, FEM simulations on first nozzle layouts were completed and nozzles were evaluated and adapted according to their suctioning behavior and generated droplet distribution with diluted photoresist (AZ9260 1:3 in PGMEA). Considerations and calculations on the simulation were accomplished taking into account results by Dagaonkar *et al* of simulations on a venturi liquid/liquid dosage system [9]. A dynamic viscosity of 0.42 mPa · s at room temperature was assumed, as the most appropriate solvent for the OSCs was yet to be determined.

Table 1. Dimension parameters of tested nozzles. Etch depth T of all nozzles was 100 μm. Droplet size is geometric mean of probability density function of dried droplets sprayed from diluted photoresist.

Nozzle	M (μm)	N (μm)	D (μm)	W (°)	L (μm)	Droplet size (μm)
2k (2.7)	50	300	100	60	0	17.81[d]
4	50	300	100	170	50	23.63
4.05	**50**	**300**	**50**	**170**	**50**	**28.68**
10	50	300	100	170	50	32.16
4b	50	500	100	170	50	32.45
2.br (2.2)	150	300	100	120	150	41.22
2	50	300	100	120	50	64.19
2k.br.05	150	300	50	60	150	69.45[e,f]
2–50 (2.1)	50	300	50	120	50	n.a.[a]
5b	50	300	50	0	50	n.a.[a]
2–25	50	300	25	120	50	n.a.[a,b]
3	50	300	100	0	300	n.a.[a,b]
9	50	500	100	120	300	n.a.[a,b]
7	50	500	100	120	300	n.a.[b,c]
2k.05	50	300	50	60	0	n.a.[c]
11	50	500	100	120	50	n.a.[c]
1	50	300	100	120	300	n.a.[c]
8	50	500	100	0	300	n.a.[c]
2k.br	150	300	100	60	0	n.a.[e]
4.br	150	300	100	170	150	n.a.[e]
4.br.05	150	300	50	170	150	n.a.[e]

[a] Lack of suction,
[b] Unsteady spraying,
[c] Low maximal pressure,
[d] Insufficient suction,
[e] Too high mass flow,
[f] Values at 8 cm distance.

Table 1 shows some of the tested nozzles with their geometric parameters, as illustrated in figure 1.

SEM pictures of the selected micronozzle design are shown in figure 2, featuring a medium inlet (a2) in an atomizing gas restriction (a1). Higher gas velocity (red arrow) caused by the smaller restriction width results in a pressure drop and a medium flow towards restriction and nozzle opening (blue arrow with broken line).

The pressure drop is dependent on the ratio of atomizing gas tube width to restriction width as well as on the width of the medium inlet. By increasing the medium inlet width, the media flow may be increased. The used design features a nozzle opening and medium inlet width of 50 μm and an atomizing gas tube width of 300 μm.

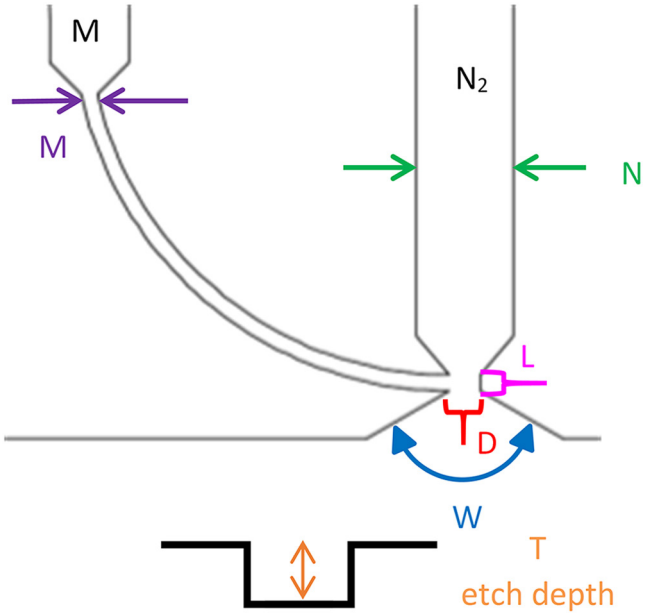

Figure 1. Illustrated nozzle dimension parameters.

2.2. Fabrication

The nozzle design was realized using photolithography (10 μm AZ9260, 208 mJ i-line) and deep reactive ion etching (DRIE) on silicon wafer substrates (phosphor doped, single side-polished (SSP)) Czochralski grown silicon wafer with a diameter of 100 $\pm$ 0.3 mm (4″), a resistivity of 5–10 $\Omega \cdot$ cm and a thickness of 525 $\pm$ 20 μm) utilizing an Oxford Plasmalab 80plus. The process was optimized by variation of exposure time, film thickness, gas chopping intervals and inductive coupled plasma (ICP) power to achieve a reproducible sidewall angle and channel depth. Furthermore, a conditioning process was found to obtain reproducible etch rates using a versatile utilized R&D RIE device. By connecting the nozzles with attached fluidports (the nozzle and fluidport body are shown in figure 2(b)) instead of glued fused silica capillary tubes, it was possible to realize the nozzles in only one etch depth, wihout requiring a connection plane with tube OD depth.

After substrate cleaning (peroxomono-sulfuric acid (140 °C, 10 min), ultrasonic 2-propanol bath (10 min)), the structured silicon wafer is capped using a glass wafer (ultrasonic cleaned (2-propanol, 10 min)), which is pre-drilled (1.2 mm in diameter) for media connection, and anodic bonding at 400 °C and 1.1 kV. The cleaning with piranha etch becomes possible here because the nozzles only consist of the crystalline silicon substrate and a glass wafer. The acid is a widely applied cleaning solution for both materials. Nozzles are then separated by wafer dicing alongside designated scribe lines (figure 3) and as mentioned connected using fluidports and a nozzle-clamping mount (figure 4(c)) to reversible clamp the fluidports tight onto the nozzles. The nozzle clamping mount, media reservoirs and perfluoroalkoxy alkane (PFA) tubings are installed on the spray head featuring a four-way L-valve for immediate after-spray flushing (figure 4(b)). The spray head is easily screwed onto the x-axis stage of the spray coater and the atomizing gas tube is connected with the nitrogen supply. The spray coater, developed and constructed at the competence center Nanochem of OTH Regensburg, is depicted in figure 4, equipped with a spray head and micronozzle. Upscaling in terms of output and coating velocity is easily possible by realizing several nozzles aligned next to each other on the wafer level, with separate inlets for atomizing gas and medium, or even by melding channels to single inlets for atomizing gas and medium. The aforementioned substrate cleaning process is also applied for nozzle cleaning after spraying, as it oxidizes and removes all organic residues contained in the organic semiconductor solution. Flushing with chlorobenzene prior to this is convenient as a pre-cleaning process.

Reproducible etch rates of 1.1 μm per step and slightly negative sidewall angles of 87–90° were achieved using a SF_6/CHF_3 Bosch process, two-precedent chamber cleaning and one conditioning process. The chamber walls were cleaned with 30/30 sccm SF_6/O_2 [10] and 50 sccm of O_2 both for 20 min at 20 mTorr, 300 W ICP power and 200 W RF forward power. Conditioning was accomplished with 150 steps of the following Bosch process on a photoresist (AZ9260) coated non-structured dummy wafer [11]. The gas flow of all process gases during the Bosch process was 100 sccm with 300 W ICP power and a turbopump valve opening of 40°. After a first 5 s strike (20 sccm SF_6/50 sccm CHF_3, 10 mTorr, 35 W forward power) pulsed Bosch etching loops consist of 5 s CHF_3-passivation (10 W forward, 90 W bias power) and 8 s SF_6-dry-etching (30 W forward, 140 W bias) separated by two 3 s purge steps with the following process gas. 100 μm etch depths were achieved by 91 loops accordingly. All processes were kept at a temperature of 20 °C. Previous results showed a resist removal of about 3.6–3.7 μm during dry etching, which corresponds to a selectivity (silicon to resist etch rate) of about 27.

2.3. Nozzle tests

2.3.1. Spray cone. To obtain an area distribution of the spray cone, P3HT/PCBM solution in chlorobenzene (1:0.75:98.25 wt%), referred to as OSC solution in the following, was sprayed on a glass substrate for defined periods of time at a constant position using the micronozzle and conventional airbrush nozzle set (Harder & Steenbeck, 0.15 mm diameter) for the purpose of comparison. Chlorobenzene with relatively low vapor pressure and high boiling point was used as the sole solvent for P3HT and PCBM in all experiments. Solvents such as chlorobenzene or dichlorobenzene (DCB) have to be deployed because the large surface of small drops greatly enhances evaporation during deposition. The spray spot was measured using a P-16 KLA Tencor profilometer.

2.3.2. Drop size. For further nozzle characterization, the OSC solution was sprayed at 7 bar on a glass substrate with a high stage velocity of 100 mm $\cdot$ s^{-1} to receive distinct droplets. The diameter of at least 1000 dried droplets (after 5 min of 140 °C annealing) was measured using optical microscopy to achieve a proper distribution. In order to receive comparable values, droplet diameter was calculated back to the drop

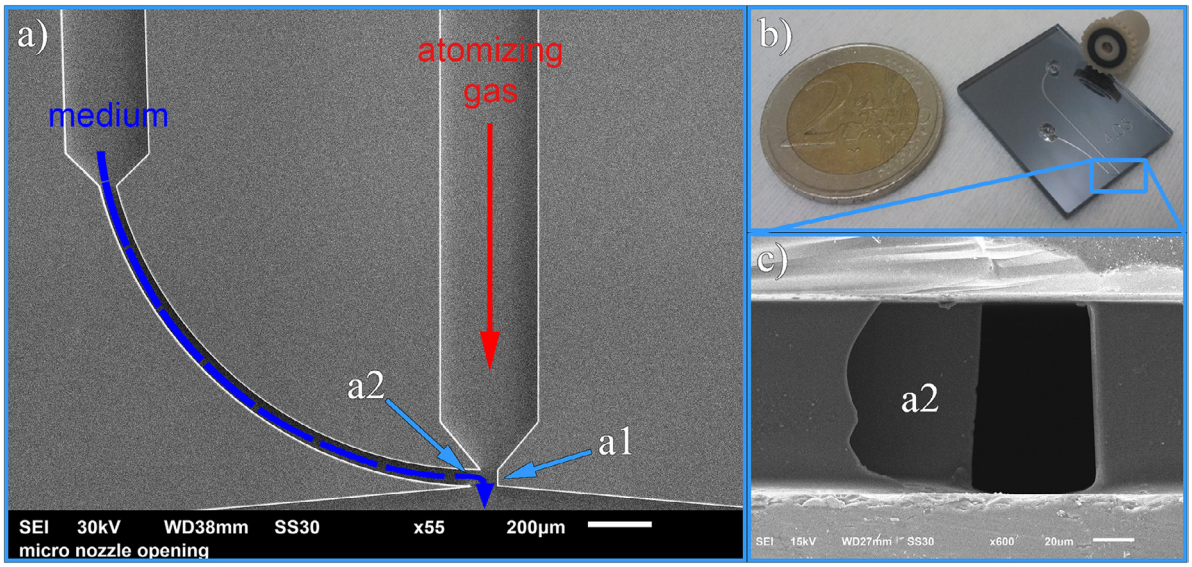

Figure 2. (a) SEM image of the nozzle layout with atomizing gas tube restriction (a1) and media inlet (a2). Fluid flow is indicated with red (atomizing gas) and blue (broken line) arrows (medium). (b) Separated nozzle with fluidport body and coin. (c) SEM image of the nozzle opening compiled from three pictures at different planes of focus.

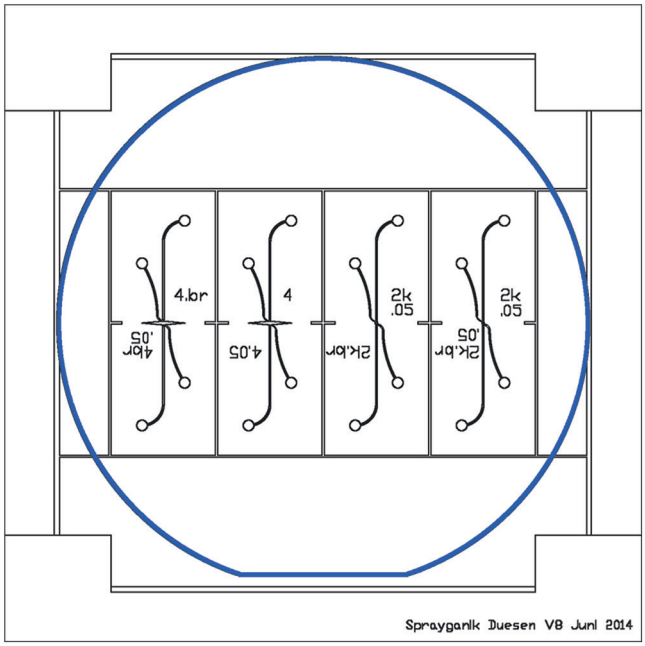

Figure 3. Photolithographic design of the overall nozzle chip with different nozzle layouts facing each other. Nozzles will be separated to 20 mm × 25 mm chips alongside plotted scribe lines. The blue shape depicts a 100 mm wafer alignable at mask openings on each side.

size with the known original chlorobenzene concentration and the droplet volume. It seems the relationship is roughly a quadratic correlation for smaller drops, while larger drops form crater-like droplets instead of flat circular ones, and show a higer degree of correlation. A dry droplet with a diameter of 9.89 μm (flat) sprayed at a distance of 3.5 cm for example shows a volume of 195.5 μm³ corresponding to a wet spherical drop diameter of 7.2 μm.

2.3.3. Atomization. In order to visualize and compare atomization, spraying was recorded for the micronozzle and the

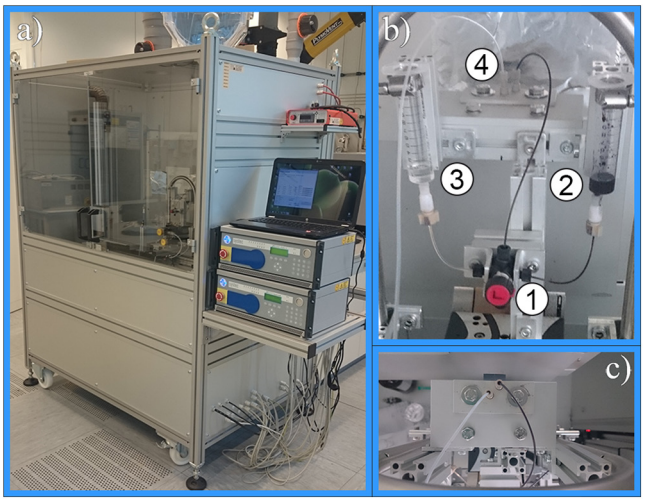

Figure 4. (a) Spray coater with acrylic spray chamber doors and control units on the right side. (b) Spray head with L valve (1), syringe barrel reservoirs for OSC solution (2), chlorobenzene (3), and clamping mount (4). All mounted on the *x* axis stage inside the spray chamber. (c) Top view of clamping mount with clamped micronozzle and connected OSC and atomizing gas tubes.

airbrush nozzle using a Photron FASTCAM SA5 high speed camera, magnification lenses and 50 W LED backlight. Both nozzles were installed and connected to the atomizing gas supply in a setup outside the spray coater to allow the placement of camera equipment.

2.3.4. Coating efficiency. Consumption of the OSC solution was determined by measuring the time for consuming a given volume represented by a defined length of the PFA supply tubing. Coating time for homogeneously coated 50 mm × 50 mm substrates was used to calculate solution consumption. Reversal points of the coating meander pattern with 1 mm spray line distance (raster) were chosen so as to just not affect sprayed layers. The total covered area was 66 mm × 66 mm and the

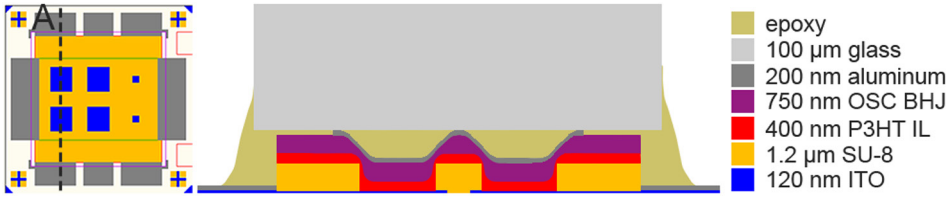

Figure 5. Diode design with cross section along cut line A.

average layer thickness was measured using the profilometer. Active volume was calculated from layer thickness and utilizable area (substrate area) and divided by the volume fraction of organic semiconductors dissolved in the coating solution to receive the coating efficiency. Calculation assumes the complete evaporation of the solvent during spray coating and the subsequent annealing. Density values of PCBM ($1.33\,g \cdot ml^{-1}$) and P3HT ($1.15\,g \cdot ml^{-1}$) are obtained from literature [12].

Spraying was performed using the best parameters for the conventional airbrush nozzle, set with higher consumption and the micronozzle to receive dry layers. To obtain reasonably thin layers, the airbrush nozzle was only opened by 125 μm (pullback length of the needle) and a high nozzle movement of $100\,mm \cdot s^{-1}$ was applied. Dry layers could be obtained at a nozzle distance of 8 cm with an atomizing gas pressure of 1 bar. The applied operating atomizing gas pressures differ strongly in value as the micronozzle requires up to 7 bar whereas the airbrush nozzle can only spray coat at a maximum pressure of ~2–3 bar. Parameters for spray coating with the micronozzle were 7 bar at smaller distances and suitable velocities (2.5 cm at $45\,mm \cdot s^{-1}$, 4.5 cm at $25\,mm \cdot s^{-1}$ and 5.5 cm at $10\,mm \cdot s^{-1}$) as this nozzle shows enhanced atomization and therefore dry layers are obtained at a much shorter nozzle distance.

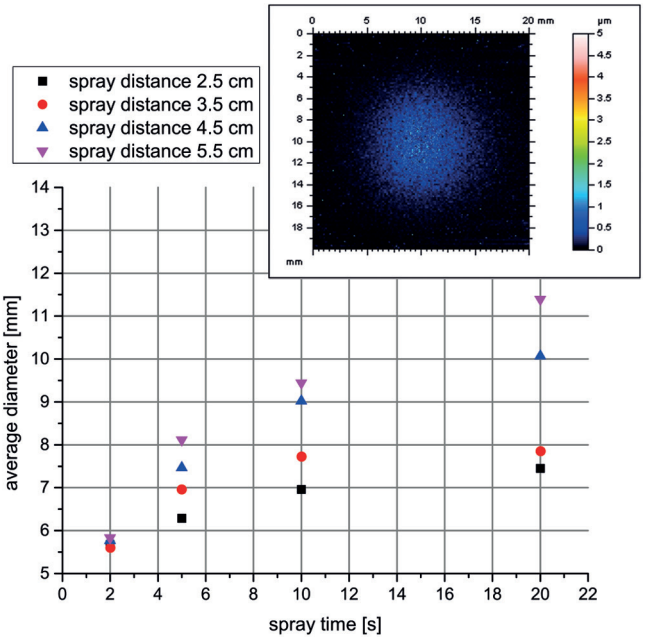

Figure 6. Spray cone diameter. Inset shows spray spot at 3.5 cm distance after 10 s of spraying. Average numerical eccentricity was 0.213.

2.4. Spray coated layers

To acquire spray parameters and evaluate spray results of the micronozzle, P3HT interlayers (to improve the hole-selectivity of the indium tin oxide (ITO) electrode [13]) and P3HT/PCBM layers were sprayed at room temperature and in section 2.3.4 tested distances and velocities to deposit layers of about 200 nm thickness per spray step. The P3HT interlayer was sprayed twice from a P3HT:chlorobenzene solution (1:99 wt%) to guarantee complete coverage of the ITO contact while accepting additional light absorption without exciton generation. P3HT with a molecular weight of 57 kg per mole, a regio-regularity of 91% and a polydispersity index of $\leqslant 2.4$ was applied (Rieke Metals LLC). The aforementioned P-16 KLA Tencor profilometer was utilized to measure cross section of the OSC layers.

Used glass substrates featured 120 nm of structured ITO as bottom electrode passivated with 1.2 μm of SU-8 photoresist. Finally, 200 nm aluminum was vapor coated as top contact and the diode was encapsulated with epoxy glue inhibiting water and oxygen diffusion. Current density was then measured over voltage (−2 V to 1 V) with and without green 532 nm irradiation ($780\,\mu W \cdot cm^{-2}$).

Figure 5 schematically shows the design and layer structure with corresponding thicknesses of a diode chip with four active areas of $10\,mm^2$ and two of $1\,mm^2$. The OSC layer forms a bulk heterojunction (BHJ) nanostructure with large interfaces between donor and acceptor [14].

3. Results and discussion

3.1. Nozzle tests

3.1.1. Spray cone. The resulting shape was a quasi-circular ellipse with an average numerical eccentricity of 0.213, though dry particles settle outside this area (figure 6). Shape broadening is observed over time as excessive medium is laterally blown away. An opening angle from 8.9 to 13.6° is calculated and most likely is about 10°, taking into account shape broadening at longer spray times and poor detectability at shorter spray times. Airbrush spraying did result in larger spray spots ranging from 14.75 mm to 20.84 mm after 5 s at distances from 5 to 11 cm, but a similar opening angle (10.59°, without a value at 5 cm due to excessive shape broadening), and average numerical eccentricity (0.216).

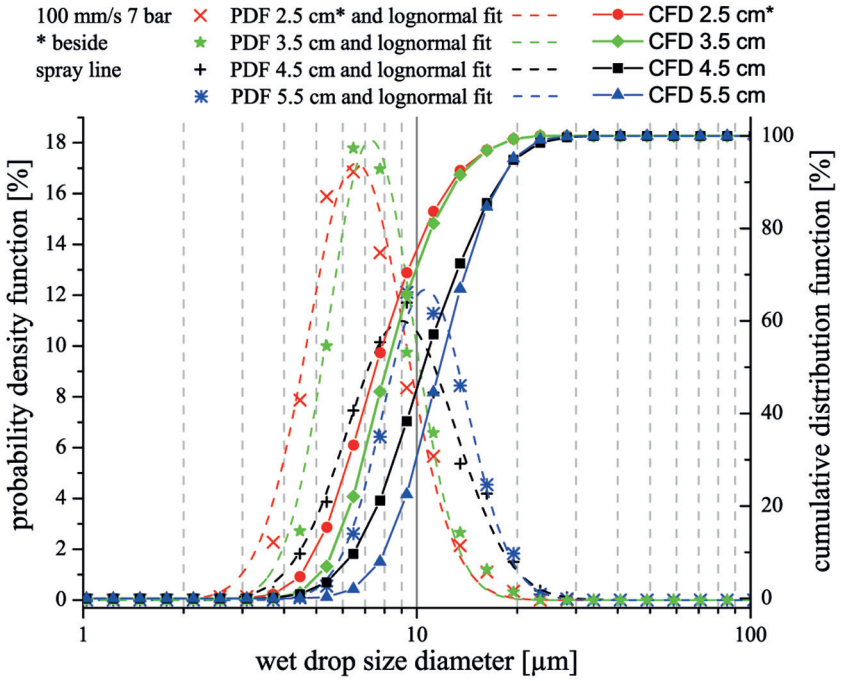

Figure 7. Probability density function (PDF) and cumulative density function (CDF) of wet drop diameters sprayed at 7 bar and 2.5, 3.5, 4.5 and 5.5 cm distance.

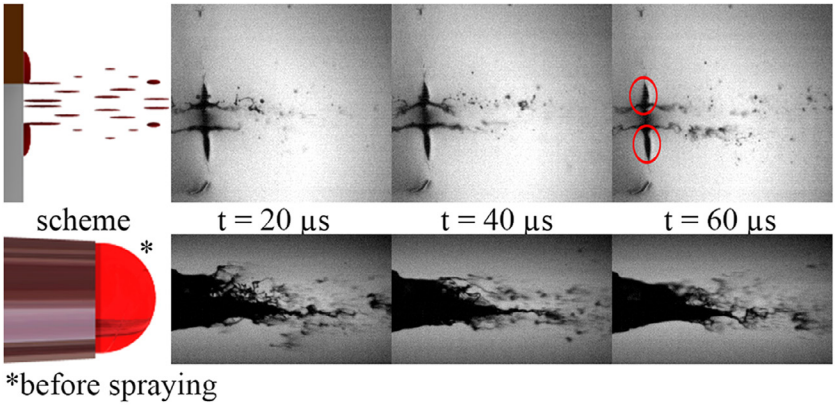

Figure 8. High-speed camera frames with $\Delta t = 20$ μs for the micro venturi and the airbrush nozzle. Tearing is visible for both nozzles. While drops next to the micro venturi nozzle opening (red circles) are drawn back into the atomizing gas stream, atomization will eventually create greater droplets resulting in observed dry particle deposition outside the dedicated spray cone. See appendix A for animated frames.

Table 2. Measured and calculated consumption values.

Tubing ID (mm)	Marked tubing length (cm)	Calculated volume (μl)	Consumption time (min:s)	Consumption ($\mu l \cdot min^{-1}$)
1.016 (0.04″)	16.65	134.99	2:37	51.59
	16.65	134.99	2:48	48.21
	16.95	137.42	4:29	30.65
4 (airbr.)	15	1884.96	1:57	1966.64

3.1.2. Drop size. The wet drop diameter follows a lognormal distribution as can be seen in figure 7. The probability density function of the drop diameter distribution shows a geometric mean of 7.4/7.9/10.4/11.6 μm (2.5/3.5/4.5/5.5 cm) and a geometric standard deviation of 1.40/1.34/1.46/1.34 μm. With increasing nozzle distance the wet drop diameter increases as well, which, in our view, might be contributed to by the agglomeration of drops.

3.1.3. Atomization. In order to investigate atomization, the spray performance was recorded with a high-speed camera. As velocities are very high and the depth of field is shallow, drops

Table 3. Calculations for coating efficiencies of micronozzle and airbrush.

Spray distance (cm)	Nozzle velocity (mm · s^{-1})	Pattern (mm^2)	Spray steps	Consumption (μl min^{-1})	Coating time (min)	Thickness (nm)	Coating efficiency (%)
3	45	66 × 66	5	51.59	12	821	20.66
3	45	**56 × 56**	5	48.21	9:20	1085	35.1
2.5	45	66 × 66	5	30.65	12:01	453	19.16
4.5	25	66 × 66	1	30.65	3:31	166	24.02
		66 × 66	5		17:35	673	19.46
5.5	10	66 × 66	1	30.65	7:37	341	22.73
		66 × 66	6		45:42	2007	22.32
8 (airbrush)	100	66 × 66	1	1966.64	1:22	741	8.74

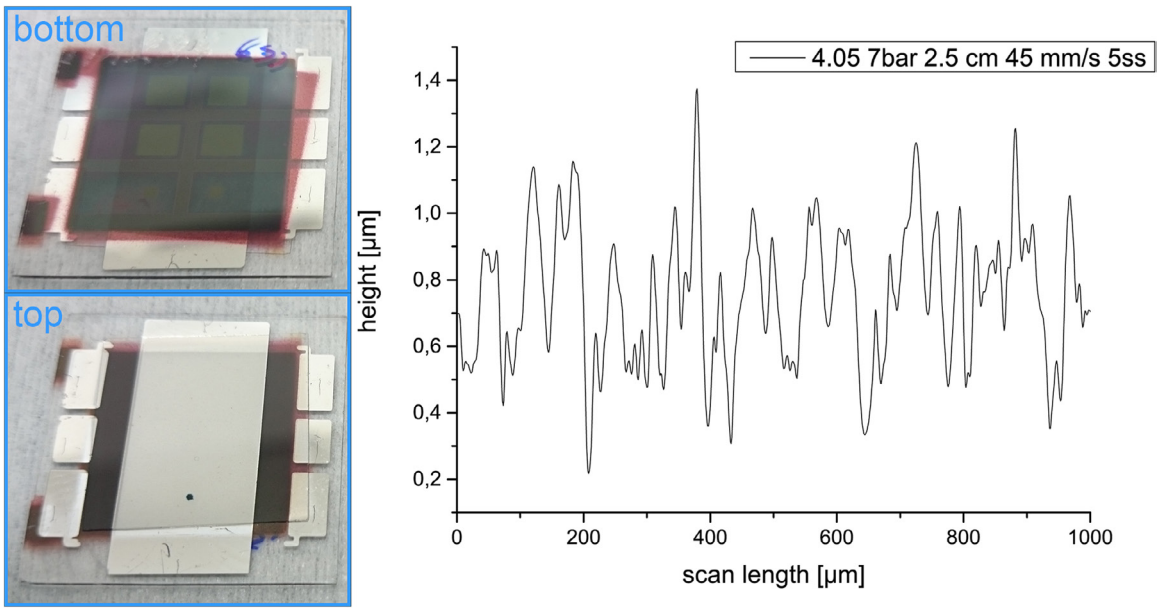

Figure 9. Photo diode device with four diodes of 10 mm^2 and two of 1 mm^2 active areas according to the design depicted in figure 5. The profile shows the organic layer with a root mean square (rms) of 206.3 nm. Subjacent layers have been subtracted but may have caused an increase in roughness.

themselves could not be visualized during flight, but constant or high frequency tearing from drops right below and above the micronozzle opening could be observed. These drops form either due to the condensing of the atomized medium or simply due to not yet atomized medium. Tearing becomes more and more frequent with higher atomizing gas pressure, resulting in quasi constant spraying at 7 bar and higher. The airbrush nozzle set also shows this pressure-dependent tearing though, at lower pressure values up to 2 bar and with higher outputs. In all cases, the medium is atomized outside of the nozzle when it enters or re-enters the atomizing gas flow. Medium drops accelerated perpendicular to the propellant flow are drawn back to the stream. Atomization inside the nozzle could not be observed by the means applied. As the 3D cone forms, spray drops move out of focus quickly and only a small part of the pictured spray cone can be visualized clearly at the same time (figure 8).

3.1.4. Coating efficiency. The determined consumption values are given in table 2. The airbrush nozzle uses a larger medium tubing and shows much higher consumption. The

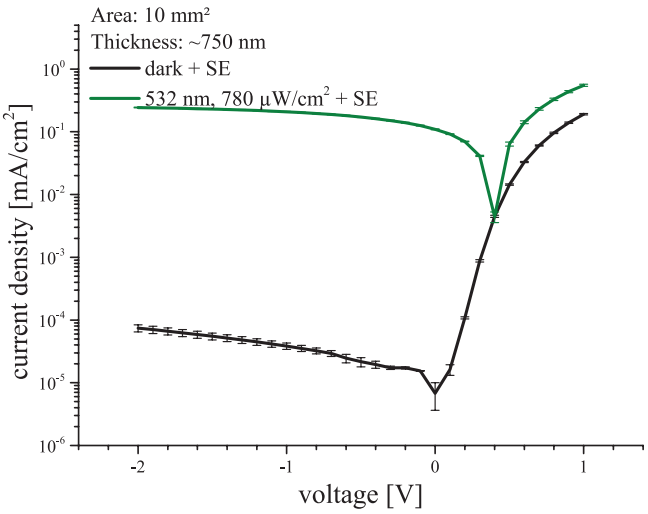

Figure 10. Current density over voltage for first sprayed diodes with a dark current (black curve) of ~7.41 · 10^{25} mA · cm^{-2} and an external quantum efficiency (EQE) of 72.9% (both measured at −2 V), calculated from the illuminated green curve. Standard deviation of the error (SE) results from averaging four diodes.

consumption of the micronozzle was approximately 50 μl $\cdot$ min^{-1} for the first experiments at 3 cm distance. When supplementing results at additional distances, a reduced consumption of just above 30 μl $\cdot$ min^{-1} was detected but similar efficiencies were achieved, as given in table 3. In our view this might be as result of reduced solvent content due to evaporation.

By measuring the time and thickness of the respective coating, the coating efficiency can be calculated as described in section 2.3.4. For all micronozzle coatings, an average efficiency of 21.39% $\pm$ 1.94% is calculated, which corresponds to a 2.45 fold increase compared to airbrush efficiency. The required amount of OSCs to achieve the same layer thickness is hence reduced by 59%, allowing economical spray coating. As the spray cone diameter using the micronozzle is smaller essentially due to the smaller nozzle distance, reversal points may be set closer to the substrate without affecting the active area. Using a 56 mm $\times$ 56 mm spray pattern, coating efficiency further increases to 35.1% and consumed volume is reduced by 75% in total (a 4.01 fold coating efficiency). The coating efficiency for large substrates should approach a theoretical maximum of ~15.16% for the airbrush nozzle set and ~44% using the micronozzle (a 2.9 fold coating efficiency) with the overlapping area of the spray pattern eventually becoming negligible. These values almost reach and considerably exceed the coating or 'transfer' efficiency of ~20% empirically determined for an ultrasonic spray nozzle [15], even though this value may vary noticeably with different nozzles.

3.2. Sprayed layers

OSC layer homogeneity decreases with greater micronozzle distance, which indicates small drops with low solvent fraction after greater distances. Droplets were distinguishable partially through transmitted optical microscopy, as further drops do not dissolve already dried subjacent droplets. Their size ranges from about 5 to 50 μm and matches the droplet size measured in section 3.1. Results are shown for the smallest nozzle distance of 2.5 cm as for greater distances with fewer spray steps, layer inhomogeneity partially resulted in nonclosed layers, which causes short circuits during electrical characterization. Even at a short distance a high roughness root mean square (rms) of 206.3 nm of the P3HT interlayer and OSC stack was measured (figure 9).

No short-circuits were detected for the small nozzle distance of 2.5 cm with a comparably high stage velocity of 45 mm $\cdot$ s^{-1} and five spray steps. *J*/*V* characteristics of 10 mm^2 active area diodes are shown in figure 10.

Current density over voltage of produced diodes shows an average dark current of 7.41 $\cdot$ 10^{-5} mA $\cdot$ cm^{-2} ($-$2 V), which is within a common magnitude for organic photodiodes, e.g. [16]. Under green illumination (532 nm, 780 μW $\cdot$ cm^{-2}), an average current density of 0.244 mA $\cdot$ cm^{-2} ($-$2 V) was measured. An EQE of 72.9% is calculated from the ratio of generated charge carriers to photons at this wavelength.

Performance is comparable to reported values of ~70% for OPDs with ~450 nm P3HT/PCBM layer at $-$5 V bias [17]. The quantum yield could be further increased by reducing the thickness of the P3HT interlayer, which absorbs light without generating charge carriers.

4. Conclusion

Micro venturi nozzles have been realized in a silicon wafer using a single dry etch process and anodic bonding. Produced nozzles featuring a rectangular nozzle opening of 50 μm width and 100 μm depth generate a quasi-circular spray cone, which is important for the overlap of spray lines in orientation-independent coating (from the spray line center gradually decreasing in thickness in all directions). The cleaning of nozzles with aggressive acids (peroxomono-sulfuric acid) and strong solvents (e.g. chlorobenzene) was easy and fast. The best spray results were achieved at a short nozzle distance as solvent evaporation is enhanced by the small drop diameter with a distance dependent geometric mean of 7.4 μm–11.6 μm. The average coating efficiency of the micronozzles was 21.39% $\pm$ 1.94% (35.1% for smaller pattern) for 25 cm^2 active area and therefore 2.45 times (4.01) higher than spraying with a conventional airbrush nozzle set. Presumably, the micro nozzles feature a more directional spray jet and a more efficient use of the atomized solution as no deposition of dry particles/dust is observed in the spray coater in contrast to spraying with the airbrush nozzle. This results in a 59% (75%) lower consumption and hence lower material costs when manufacturing organic photovoltaic or organic photodiodes. To achieve a sufficient coating speed, multiple nozzles or nozzle arrays may be deployed. Diodes produced from sprayed P3HT/PCBM organic semiconductor layers show state-of-the-art performance with a comparably low dark current of ~7.41 $\cdot$ 10^{-5} mA $\cdot$ cm^{-2} and an external quantum efficiency of 72.9% at 532 nm, both measured at $-$2 V. Performance may even be improved and layer thickness minimized by optimization of solution and solvent (e.g. DCB) and higher atomizing gas pressure. It is reported that layer roughness may be considerably decreased by subsequent solvent coating steps [18, 19] and that this is likely compatible to continuous, e.g. roll-to-roll, processing [20]. To improve the variance of the drop size distribution and reduce drop formation as seen in figure 8, a design with a central medium channel and surrounding atomizing gas channels is being tested at present.

Acknowledgment

We would like to thank the German Federal Ministry for Education and Research (BMBF) for funding this work (FHProfUnt grant 03FH040PX2). Furthermore, we would like to thank the Georg-August University Göttingen for providing the high-speed camera and related optical equipment.

Appendix A

Spraying of the airbrush nozzle was recorded at 50k fps and is replayed at 10 fps.

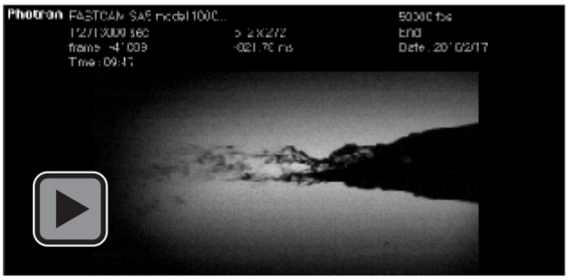

Spraying of the micronozzle was recorded at 50k fps and is replayed at 10 fps (stacks.iop.org/JMM/27/015019/mmedia).

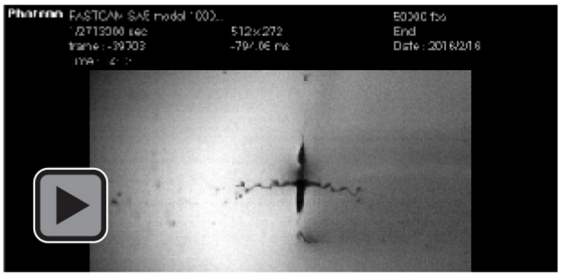

References

[1] Sargent E H 2009 Infrared photovoltaics made by solution processing *Nat. Photon.* **3** 325–31

[2] Girottoa C, Rand B P, Genoe J and Heremans P 2009 Exploring spray coating as a deposition technique for the fabrication of solution-processed solar cells *Sol. Energy Mater. Sol. Cells* **93** 454–58

[3] Krebs F C 2009 Fabrication and processing of polymer solar cells: A review of printing and coating techniques *Sol. Energy Mater. Sol. Cells* **93** 394–412

[4] Lee J H, Yoshikawa S and Sagawa T 2014 Fabrication of efficient organic and hybrid solar cells by fine channel mist sprayc oating *Sol. Energy Mater. Sol. Cells* **127** 111–21

[5] Brabec C J and Durrant J R 2008 Solution-processed organic solar cells *MRS Bull.* **33** 670–5

[6] Sigma-Aldrich Co. LLC 2015 Sigma-Aldrich (www.sigma-aldrich.com/catalog/product/aldrich/684449?lang=de&region=DE) (accessed 28 June 2015)

[7] Richter T 2012 Zerstäuben von Flüssigkeiten—Düsen und Zerstäuber *Theorie und Praxis* ed W J Bartz *et al* (Renningen: Expert Verlag) pp 112–3

[8] Arai M, Terao K, Suzuki T, Simokawa F, Oohira F and Takao H 2012 Air-flow based multifunctional tactile display device with multi-jet integrated micro venturi nozzle array *IEEE 25th Int. Conf. on Micro Electro Mechanical Systems (MEMS) (Paris)* pp 148–51

[9] Dagaonkar M, Kumaran V, Venkataraghavan R and Franklin D C 2012 Comsol.com (www.comsol.de/paper/download/153065/dagaonkar_abstract.pdf) (accessed 28 June 2015)

[10] Cunge G, Pelissier B, Joubert O, Ramos R and Maurice C 2005 New chamber walls conditiontioning and cleaning strategies to improve the stability of plasma process *Plasma Sources Sci. Technol.* **14** 599

[11] Dittmer M 2015 Optimierung der mikrotechnologischen Prozesse zur Herstellung von Mikrosprühdüsen Regensburg (self published)

[12] Kiel J W, Kirby B J, Majkrzak C F, Maranvillec B B and Mackay M E 2010 Nanoparticle concentration profile in polymer-based solar cells *Soft Matter* **6** 641–6

[13] Liang C W, Su W F and Wang L 2009 Enhancing the photocurrent in poly(3-hexylthiophene)/[6,6]-phenyl C61 butyric acid methyl ester bulk heterojunction solar cells by using poly(3-hexylthiophene) as a buffer layer *Appl. Phys. Lett.* **95** 133303

[14] Kalita M and Koichi U M 2010 Nanostructured morphology of P3HT:PCBM bulk heterojunction solar cells *Solid-State Electron.* **54** 447–51

[15] Pham N P, Burghartz J N and Pasqualina M S 2005 Spray coating of photoresist for pattern transfer on high topography surfaces *J. Micromech. Microeng.* **15** 691–7

[16] Ramuz M, Bürgi L and Seitz W C 2008 High sensitivity organic photodiodes with low dark currents and increased lifetimes *Org. Electron.* **9** 369–76

[17] Tedde S F, Kern J, Sterzl T, Fürst J, Lugli P and Hayden O 2009 Fully spray coated organic photodiodes *Nano Lett.* **9** 980–3

[18] Park H Y, Kim K, Kim D Y, Choi S K, Jo S M and Jang S Y 2011 Facile external treatment for efficient nanoscale morphology control of polymer solar cells using a gas-assisted spray method *J. Mater. Chem.* **21** 4457–64

[19] Steirer K X *et al* 2009 Ultrasonic spray deposition for production of organic solar cells *Sol. Energy Mater. Sol. Cells* **93** 447–53

[20] Steirer K X *et al* 2009 Advancing spray deposition for low-cost solar cell production *SPIE Newsroom* (doi: 10.1117/2.1200903.1555)